Analyst

RSC Publishing

COMMUNICATION

View Article Online
View Journal | View Issue

Cite this: *Analyst*, 2013, **138**, 6732

Analysis of single algal cells by combining mass spectrometry with Raman and fluorescence mapping†

Stephan R. Fagerer,‡[a] Thomas Schmid,‡[a] Alfredo J. Ibáñez,[a] Martin Pabst,[a] Robert Steinhoff,[a] Konstantins Jefimovs,[b] Pawel L. Urban[c] and Renato Zenobi*[a]

Received 7th June 2013
Accepted 20th August 2013

DOI: 10.1039/c3an01135f

www.rsc.org/analyst

In order to investigate metabolic properties of single cells of freshwater algae (*Haematococcus pluvialis*), we implement matrix-assisted laser desorption/ionization mass spectrometry (MALDI-MS) in combination with microspectroscopic mapping. Straightforward coupling of these two detection platforms was possible thanks to the self-aliquoting properties of micro-arrays for mass spectrometry (MAMS). Following Raman and fluorescence imaging, the isolated cells were covered with a MALDI matrix for targeted metabolic analysis by MALDI-MS. The three consecutive measurements carried out on the same cells yielded complementary information. Using this method, we were able to study the encystment of *H. pluvialis* – by monitoring the adenosine triphosphate (ATP) to adenosine diphosphate (ADP) ratio during the build-up of astaxanthin in the cells as well as the release of β-carotene, the precursor of astaxanthin, into the cytosol.

Studies of cellular dynamics are conventionally performed on samples composed of large numbers of cells. However, there are many scenarios where such a bulk analysis may obscure important information; for example, when studying rare cells, cells switching between *on*/*off* states, or bistable populations. Such scenarios have recently been discussed in the literature.[1,2] Consequently, the field of single-cell analysis has seen remarkable progress within the last decade, especially using ultra-sensitive techniques such as laser-induced fluorescence and mass spectrometry to detect biomolecules down to atto- and yoctomole levels.[3–5] It has also been recognized that multiparameter analysis is necessary for studying dynamic processes in single cells.[6] Hu *et al.*, for example, correlated the protein fingerprint with the cell cycle stage by combining capillary electrophoresis with fluorescent staining techniques.[7]

In this article, we demonstrate a single-cell approach combining Raman and fluorescence mapping with matrix-assisted laser desorption/ionization mass spectrometry (MALDI-MS) to analyse the encystment process of the algal species *Haematococcus pluvialis*.

H. pluvialis is a freshwater alga that may undergo a drastic morphological transformation from a motile, green form to deeply red, dormant cysts (Fig. 1A) when confronted with salt stress, strong light irradiance, or lack of nutrients.[8] This transition is accompanied by the accumulation of large quantities of astaxanthin (3,3′-dihydroxy-β,β-carotene-4,4′-dione) within the cell.[9] The red pigment is a very effective anti-oxidant and therefore of great interest to the food supplement industry. In addition, it is also employed as a dye for salmon products. Since this algal species is by far the most efficient source of astaxanthin, there is considerable interest in the biochemical synthesis of astaxanthin in order to optimise the harvest by biotechnological production.[8,10–13]

Studying encystment on the level of single cells is vital for a precise assessment of its mechanism. While a general shift in the metabolism and in the pigmentation of a cell culture can be monitored along the time axis of an applied stressor (*i.e.* lack of nutrients), the culture will always consist of cells at various stages of the encystment cycle, *i.e.* also contain young, motile green cells when the majority of the culture has already entered the immotile cyst stage. Bulk analysis of such heterogeneous cell populations may not yield representative results for the various stages of encystment and may therefore give rise to inaccurate conclusions on the mechanism. A possible solution to this problem is the separation of cells in different encystment stages by the amount of astaxanthin as a defining parameter using an optically activated cell sorting system. This method is costly and time consuming. However, microscopic Raman imaging of single cells has already been reported for single *H. pluvialis* cells in the cyst stage as well as prior stages.[14,15] Furthermore, a multidimensional chemical analysis of *Euglena*

[a]*ETH Zürich, Wolfgang-Paulistr. 10, Zürich, Switzerland. E-mail: zenobi@org.chem.ethz.ch; Fax: +41 44 632 1292; Tel: +41 44 633 4838*

[b]*EMPA (Swiss Federal Laboratories for Material Science and Technology), Überlandstr. 129, Dübendorf, Switzerland*

[c]*National Chiao Tung University, 1001 University Rd, Hsinchu City, 300, Taiwan*

† Electronic supplementary information (ESI) available. See DOI: 10.1039/c3an01135f

‡ Contributed equally

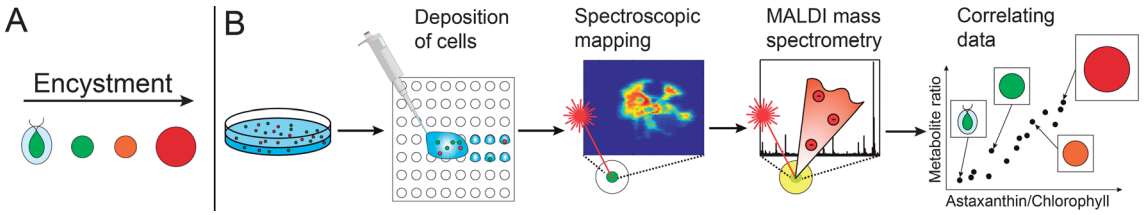

Fig. 1 (A) Schematic representation of morphological changes during encystment of *H. pluvialis*. (B) The proposed single-cell approach for combined analysis of metabolites using multiple analytical platforms.

gracilis has already been performed in our group.[16] Therefore, it is appealing to apply this multidimensional analysis approach (that includes mass spectrometry and microspectroscopies) in dynamic profiling of heterogeneous *H. pluvialis* cell populations (Fig. 1B).

Experimental section

The *H. pluvialis* algal cells (strain 34-1b, EPSAG Goettingen, Germany) were grown in 20 mL Algro medium (Carolina biological supply, Burlington, North Carolina, USA) inside Petri dishes during several weeks. The culture was illuminated with a source of white light (8 μmol photons per m^2 per s or 600 lux). Samples were collected every few days in order to obtain cells at various stages of encystment. The cells were stressed by nutrient limitation. Prior to analysis, the suspension of sampled cells was diluted in 1 : 5 (v/v) ratio with cold (0 °C) deionized water in order to quench the metabolism. Different washing procedures were tested to remove salts from the suspension but we found that the dilution protocol yielded similar spectrum quality when compared to washing protocols. Furthermore, mere dilution did not expose the cells to osmotic stress or centrifugation.

The cells were isolated using micro-arrays for mass spectrometry (MAMS) – a technology developed previously in our group.[17] MAMS targets feature an array of hydrophilic spots in an omniphobic environment which allows for aliquoting of pico- to nanoliter sized droplets. In brief, MAMS chips are produced by coating rectangular indium-tin oxide covered glass slides (75 × 25 mm, resistivity 15–25 Ω per square, Sigma-Aldrich, Buchs, Switzerland) with an omniphobic layer of polysilazane (Eposint, Pfyn, Switzerland). Then, an array of 13 × 13 hydrophilic, circular spots with a diameter of 100 μm is created by ablation with a femtosecond laser (EMPA, Dübendorf, Switzerland) as shown in Fig. S1.† The cells were isolated by dragging a 5 μL droplet of a cell suspension across the hydrophilic reservoirs. In this way, a small number of single cells can be separated (typically 0–4 cells per reservoir, with an approximate yield of 5% for single-cell spots). The unique address of each array position allows for the unambiguous recovery of each single cell. The positions of individual cells were identified using a microscope (Zeiss, Germany) and then transferred onto the Raman/fluorescence setup.

Raman and fluorescence mapping was performed with a commercial Raman/fluorescence setup (NT-MDT, Moscow, Russia). The glass slide was positioned on a manual *xy* stage and the reservoirs containing single cells were approached one by one. A laser with a wavelength of 532 nm and a power of 50 μW at the sample was employed. Typically, an image raster of 64 × 64 pixels at a pixel size of 500 nm × 500 nm was used for both Raman and fluorescence microspectroscopy. Raman spectra in each pixel were recorded from 0 to 2500 cm^{-1} within 100 ms. The fluorescence spectra were collected from 455 nm to 780 nm within 20 ms. Typical spectra are shown in the ESI (Fig. S2 and S3†). The estimation of the total chlorophyll and astaxanthin signal per cell was performed by integrating over all pixels of the image after background subtraction.

Following the microspectroscopic analysis, the cells were covered with a layer of the MALDI matrix 9-aminoacridine, which has already been reported to be useful for very sensitive detection of phosphorylated metabolites, and is very suitable for the analysis of primary energy metabolism-related metabolites.[3,18] It was found that the method of the MALDI matrix application was essential to the successful detection of metabolites. In the past, we successfully employed spraying protocols for yeast cells (ultrasonic transducers or airbrush application of matrix).[5,19] However, for this organism we found that deposition with a syringe pump connected to a fused silica capillary (160 μm o.d., 20 μm i.d.) and a movable sample stage allows for the localized, cross-contamination free deposition of the matrix (Fig. S4†). We used a concentration of 2 mg mL^{-1} 9-aminoacridine in a 9 : 1 (v/v) mixture of acetone and water. The solvent composition was optimized to give a bed of small, uniform crystals (see ESI†). The wet application of the matrix – in contrast to the much drier spraying protocols – allowed for good homogeneous co-crystallization. Typically, ~80 nL of the matrix were deposited into every reservoir of the MAMS chip. The hydrophobic coating greatly improved the matrix loading process since the matrix (while still in solution) contracted into the circular spots.

MALDI-MS was performed using an ABI 4800 MALDI-ToF/ToF instrument (AB Sciex, Framingham, USA) in the negative-ion reflectron mode. The software of the ABI 4800 MALDI includes an editor that allows to teach the spot set geometry of a given MALDI target to the instrument. There, the layout, shape and size of the spots were defined. After the chip was aligned in the instrument using the corner points of the array, the software allows for approaching specific addresses. When analyzing a spot, a randomized search pattern of 200 positions with each 200 laser shots was applied in order to accumulate a final spectrum. Considering the diameter of the laser focus (30 μm) and of a reservoir (100 μm), it is safe to assume that the whole spot is evenly covered by MALDI shots. The *m/z* range was set to

150–900. The laser power was ~2 × 10^8 W cm^{-2}. Data processing was done using our own code in MATLAB (Mathworks, USA) for MS peak extraction, Raman and fluorescence background correction and plotting.

Results and discussion

Microspectroscopic mapping

Mapping cells yielded the signals of β-carotene, astaxanthin, chlorophyll A, and – in their motile form – also chlorophyll B. In the Raman spectrum, the characteristic peaks of β-carotene and astaxanthin are distinguished based on a wavenumber difference of 10 cm^{-1} (1530 *vs.* 1520 cm^{-1}).[20] Chlorophyll A and B had a maximum of emission at 680 and 600 nm, respectively.

By analysing the spatial distribution of both chlorophyll and astaxanthin (or its precursor β-carotene) in an unstressed and a stressed cell we were able to track the liberation of β-carotene into the cytosol (Fig. 2). In Fig. 2D chlorophyll and β-carotene are co-localized. It is known that carotenoids accumulate in association with the photosynthetic complexes in the chloroplast membranes.[21] However, the conversion of β-carotene to astaxanthin is completed outside of the chloroplasts in cytosol. Fig. 2L and P show that – in the cells at a later stage of encystment – the carotenoid is spread across the whole cytosol. It has been hypothesized that the enzymes required for oxygenation and oxidation are only available in the cytosol and therefore the liberation is necessary for the synthesis of astaxanthin (Fig. S5†).[21]

Mass spectrometry

The mass spectra recorded with our method show numerous peaks featuring high signal-to-noise ratios and minimal matrix interference. In Fig. 3 a mass spectrum of a motile, green cell is shown. A table of signals can be found in the ESI (Table S1†) in addition to zoomed segments (Fig. S6†) and MS/MS spectra (Fig. S7†). We found specifically that cells at the last stage of encystment (which can be identified by their large size and deep red color, see Fig. 1A) did not give detectable signals. A possible explanation is the known fact that most of their biomass in this stage consists of apolar ketocarotenoids[8] which do not ionize well. Furthermore, it has been reported that photosynthetic activity is decreased, which in turn affects levels of primary metabolites.[21] It has also been reported that cysts possess thick, crystalline cell walls.[22] We tested whether the strong glycoprotein enforced membrane impedes the liberation and ionization of metabolites from the cell. We used a cell mill (Potter homogenizer, Braun Biotech International) to lyse cells on the

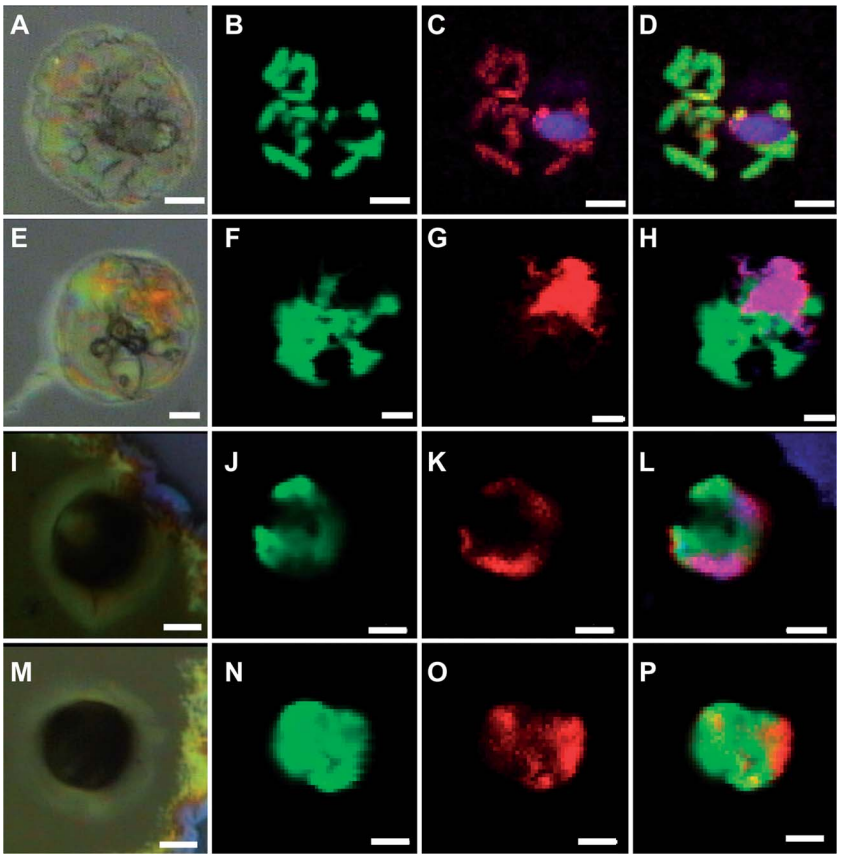

Fig. 2 Raman and fluorescence mapping of single cells found in different encystment stages: an unstressed (A–D) *H. pluvialis* cell, an intermediate stage of encystment (E–H) and cysts (I–P). (A), (E), (I) and (M) show a microscopic image of the cell. (B), (F), (J) and (N) show a fluorescence signal at 680 nm (green) corresponding to chlorophyll A. (C) and (D) also show the fluorescence signal of chlorophyll B (600 nm, purple). (C), (G), (K) and (O) show the distributions of β-carotene (1530 cm^{-1}, (C), red) and astaxanthin (1520 cm^{-1}, (G), (K) and (O), red). (D), (H), (L) and (P) show overlays of the Raman and fluorescence maps. All scale bars correspond to 5 μm.

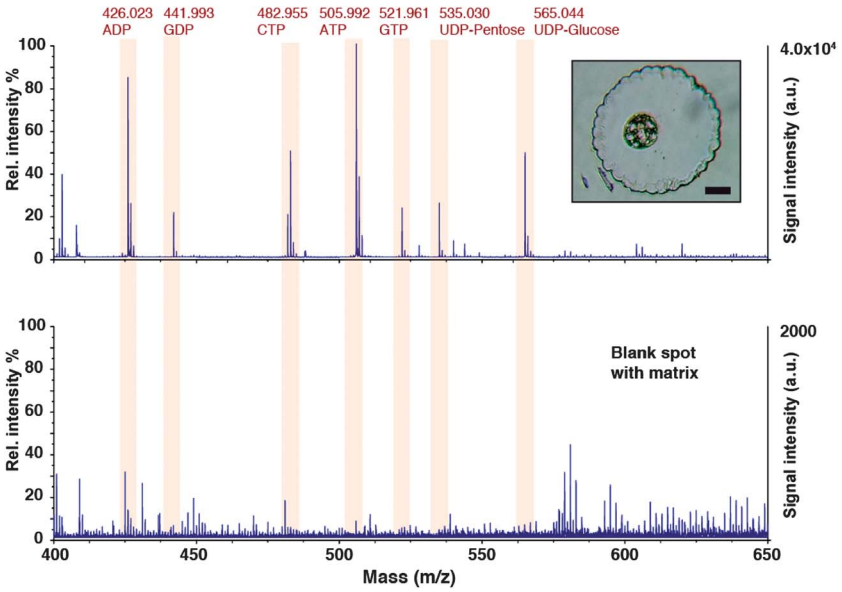

Fig. 3 Mass spectrum of a single *H. pluvialis* cell (top) and a neighboring blank reservoir (bottom). The inset shows the measured cell in a well of the MAMS chip prior to matrix deposition. The scale bar corresponds to 20 μm.

population level (500 cells per μL). The lysate was mixed with 9-aminoacridine spotted on a MALDI plate. None of the phosphorylated metabolites were detected (Fig. S8†), indicating that metabolite levels are indeed very low, below the limit of detection of our method.

Combination of microspectroscopic mapping and mass spectrometry

By overlaying the levels of information gathered from spectroscopy and mass spectrometry it was possible to reveal metabolic events during progressing encystment, the latter being indicated by the accumulation of astaxanthin. Using the data acquired for 10 single-cell samples, we correlated the ATP/ADP ratio (which can be regarded as a proxy for the cell's "energy charge") with the astaxanthin/chlorophyll ratio (Fig. 4). The exact formula for the energy charge[23] was not used due to the fact that AMP could not be detected for some of the sampled cells. Employing intensity ratios rather than intensities was advantageous for the spectroscopic mapping since local sample variations (*e.g.* reflectivity) and day-to-day variation of the laser power are eliminated. The graph in Fig. 4 shows that the ATP/ADP ratio drops with increasing astaxanthin content. This indicates the dynamic progress of encystment. It has been shown that although the concentration of chlorophyll is stable, the photosynthetic activity decreases during encystment due to damage to the photosynthetic system.[24,25] Specifically, damage to the photosystem II and low cytochrome *f* concentration are considered responsible for the decrease in efficiency of photosynthesis. This inevitably affects levels of energy-related metabolites, as well as the ATP/ADP ratio. However, since the cells are entering a dormant state, one would intuitively assume that high energy levels are not required for survival. It is important to note that the correlation of metabolites with increasing encystment is only possible using single cells because an asynchronous cultured population consists of cells at various encystment stages. Other metabolites and metabolite ratios did not show clear trends in analogous plots, which indicates that the drop of energy charge is the most pronounced reflection of the physiological transformation in the metabolism. In Fig. 4, one can notice that one of the studied cells does not fall into the trend set by other cells, showing a high ATP/ADP ratio in relation to its astaxanthin/chlorophyll ratio. Such "outliers" are very interesting for biological studies since many phenomena, *e.g.* bacterial resistance to antibiotics/stress, are based on a rare, differing behaviour of few cells or even a single cell.[26] Using microarrays with very high numbers of spots (>1000) it should be possible to study such outliers more in-depth.

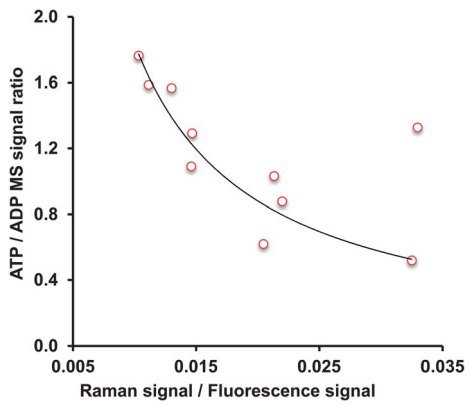

Fig. 4 Integration of data values obtained with three different techniques for the same individual cells. ATP/ADP ratios (by mass spectrometry) of all measured cells plotted against their astaxanthin/chlorophyll content (represented by the Raman signal at 1520 cm^{-1} and the fluorescence at 680 nm). The black line was added as a visual aid and does not represent a fit.

Conclusions

We have demonstrated an approach for dynamic analysis of single cells combining optical spectroscopy and MALDI mass spectrometry. Using Raman and fluorescence micro-spectroscopic mapping (at a resolution of 500 nm), it was possible to reveal biosynthesis of β-carotene in chloroplasts, and subsequent release to cytosol for biotransformation to astaxanthin. Moreover, using MAMS technology, we were able to detect 13 metabolites with high signal-to-noise ratios in single cells. Finally, by correlating these two layers of information, it was possible to show the decline of the ATP/ADP ratio during the accumulation of astaxanthin. Obtaining such correlations between abundances of primary and secondary metabolites within populations of single cells is very difficult using other methodologies. The result is in good agreement with the literature[21] and shows that the method works in practice. We believe that the method may be applied to study other dynamic cellular processes (*e.g.* cell development) in order to provide new insights into their mechanisms. Next to fundamental biological research, this single-cell analysis technique may help in developing biotechnological processes involving algae farming, *e.g.* for the evaluation of the metabolic efficiency of algae strains. Adding automation to the analytical workflow and implementing chips with a high number of reservoirs will enable the collection of multidimensional data for hundreds of MAMS-aliquoted cells, thus facilitating future biology-oriented studies.

Acknowledgements

We thank Klaus Eyer for the preparation of the lysed cell sample and Jasmin Krismer for valuable discussions. This project was co-financed by the Swiss KTI (Kommission für Technologie und Innovation), grant no. 13123.1 PFNM-NM. We also thank ABSciex for the loan of an ABI 5800 MALDI ToF.

Notes and references

1 M. E. Lidstrom and D. R. Meldrum, *Nat. Rev. Microbiol.*, 2003, **1**, 158–164.
2 D. Di Carlo and L. P. Lee, *Anal. Chem.*, 2006, **78**, 7918–7925.
3 A. Amantonico, J. Y. Oh, J. Sobek, M. Heinemann and R. Zenobi, *Angew. Chem., Int. Ed.*, 2008, **47**, 5382–5385.
4 R. Trouillon, M. K. Passarelli, J. Wang, M. E. Kurczy and A. G. Ewing, *Anal. Chem.*, 2013, **85**, 522–542.
5 P. L. Urban, A. M. Schmidt, S. R. Fagerer, A. Amantonico, A. Ibanez, K. Jefimovs, M. Heinemann and R. Zenobi, *Mol. BioSyst.*, 2011, **7**, 2837–2840.
6 D. G. Spiller, C. D. Wood, D. A. Rand and M. R. H. White, *Nature*, 2010, **465**, 736–745.
7 S. Hu, L. Zhang, S. Krylov and N. J. Dovichi, *Anal. Chem.*, 2003, **75**, 3495–3501.
8 S. Boussiba and A. Vonshak, *Plant Cell Physiol.*, 1991, **32**, 1077–1082.
9 C. D. Whitmore, U. Olsson, E. A. Larsson, O. HindsgaU, M. M. Palcic and N. J. Dovichi, *Electrophoresis*, 2007, **28**, 3100–3104.
10 M. R. Droop, *Arch. Microbiol.*, 1955, **21**, 267–272.
11 M. Kobayashi, T. Kakizono and S. Nagai, *Appl. Environ. Microbiol.*, 1993, **59**, 867–873.
12 M. Kobayashi, Y. Kurimura and Y. Tsuji, *Biotechnol. Lett.*, 1997, **19**, 507–509.
13 U. Tripathi, R. Sarada, S. R. Rao and G. A. Ravishankar, *Bioresour. Technol.*, 1999, **68**, 197–199.
14 A. Kaczor and M. Baranska, *Anal. Chem.*, 2011, **83**, 7763–7770.
15 A. M. Collins, H. D. T. Jones, D. X. Han, Q. Hu, T. E. Beechem and J. A. Timlin, *PLoS One*, 2011, **6**.
16 P. L. Urban, T. Schmid, A. Amantonico and R. Zenobi, *Anal. Chem.*, 2011, **83**(5), 1843–1849.
17 P. L. Urban, K. Jefimovs, A. Amantonico, S. R. Fagerer, T. Schmid, S. Madler, J. Puigmarti-Luis, N. Goedecke and R. Zenobi, *Lab Chip*, 2010, **10**, 3206–3209.
18 R. L. Vermillion-Salsbury and D. M. Hercules, *Rapid Commun. Mass Spectrom.*, 2002, **16**, 1575–1581.
19 A. J. Ibanez, S. R. Fagerer, A. M. Schmidt, P. L. Urban, K. Jefimovs, P. Geiger, R. Dechant, M. Heinemann and R. Zenobi, *Proc. Natl. Acad. Sci. U. S. A.*, 2013, **110**(22), 8790–8794.
20 A. Kaczor, K. Turnau and M. Baranska, *Analyst*, 2011, **136**, 1109–1112.
21 S. Boussiba, *Physiol. Plant.*, 2000, **108**, 111–117.
22 C. Hagen, S. Siegmund and W. Braune, *Eur. J. Phycol.*, 2002, **37**, 217–226.
23 D. E. Atkinson and G. M. Walton, *J. Biol. Chem.*, 1967, **242**, 3239–3241.
24 I. Zlotnik, A. Sukenik and Z. Dubinsky, *J. Phycol.*, 1993, **29**, 463–469.
25 S. Tan, F. X. Cunningham, M. Youmans, B. Grabowski, Z. Sun and E. Gantt, *J. Phycol.*, 1995, **31**, 897–905.
26 A. Aertsen and C. W. Michiels, *Crit. Rev. Microbiol.*, 2004, **30**, 263–273.

